Samkele Tfwala · Chia-Ling Huang · Ching-Ying Tsou · Su-Chin Chen

A landslide ternary diagram for geometric form and topographic site in Taiwan

Abstract The number of natural disasters induced by rainfall events in Taiwan has soared, with typhoons and torrential rains invariably inducing major landslides. In this study, data on major rainfall-generated landslides (605 in total) which occurred between 2006 and 2014 were used to classify landslides as types: shallow landslides (SL, 495), large landslides (LL, 34), and debris flows (DF, 76). LL were defined as landslides having an area, depth, and volume greater than 10 ha, 2 m and 2×10^5 m³, respectively. These were then analysed for their geometric form, geographic distribution, and scale and volume characteristics through a ternary diagram. A significant linear trend was found between the length (L) and volume (V) of SL, with the trend gradually moderating and converging with LL as length increased. The volume of LL displayed a significant increasing trend with depth (H), while SL and DF had less depth and average distribution. The median landslide length/width (L/W) ratios of SL and LL were quite close, and they had relatively similar morphologies; however, SL tended to occur near the slope toe, while large LL, due to their large volume, originated near the mountain ridges and extended to the nearest streams. The power law scaling components of W (β_1) and L (β_2) of SL were similar because of their (SL) small size, and they were highly concentrated at the centre of the developed ternary diagram. Through logistic regression, we further validated the exponents in classifying the landslides; β_1, β_2, and β_3 (power law scaling component of H) are used in the ternary diagram. Overall, β_1 was found to be the best model for classifying DF, SL, and LL having a correct rate of 0.955 and a lowest Akaike information criterion (AIC), 136.115, and Bayesian information criterion (BIC), 153.736. β_3, the depth index, though had a poor AIC, was 100% correct in classifying LL.

Keywords Slope failure · Geometric form index · Shallow landslides · Large landslides · Debris flows

Introduction

Seeking to shed light on the characteristics of landslides, numerous papers in the literature have examined the features of landslide movement and have proposed such forms as falls, topples, slides, translation, lateral spread, and flows (Hutchinson 1988; Cruden and Varnes 1996), where flow is the characteristic movement of debris flows. Borgomeo et al. (2014) and Bordoni et al. (2018) found that landslides generally occurred where the slope was > 10°, with falls usually occurring on 45° - 90° slopes, rotational slides largely on 15°–40°, and planar on 30°–70° slopes. Debris flows (DF) typically occur on slopes < 30°. Taiwan is very susceptible to slope-failure disasters due to her complex geomorphology and seismic activity. Mountainous terrain with steep slopes and large elevation differences occupies roughly 75% of the island, and the geology is fragile. Due to even greater geological fragility following earthquakes, and torrential rainfall induced by climate abnormalities, there has been a wide spread of landslides. In recent years, due to increased extreme rainfall events, there have been a growing number of large-scale landslides. Jacobs et al. (2017) among several other researchers have reported landslides associated with extreme rainfall events in the Rwenzori Mountains in Uganda; Bordoni et al. (2018) in Oltrpo, Italy; Dille et al. (2019) in DR Congo etc. These landslides have been broadly classified into either shallow or large landslides. Shallow landslides (SL) have a shallow slip plane, and typically small surface dimensions and a relatively short-distance movement (Santacana et al. 2003; Giannecchini 2006; Chigira and Yagi 2006). Most are induced by river or road cutting. On the contrary, large landslides (LL) are induced by gravitational slope deformation, and are thought to be a common manifestation of a creep, and have a relatively deep slip plane (Hutchinson 1988; Dille et al. 2019). Tamura et al. (2008) define deep-seated landslides as having an area greater than 10 ha or depth greater than 10 m or volume greater than 1×10^5 m³. In this study, we defined large landslides in an almost similar manner except that LL were defined as having a depth greater than 2 m and volume greater than 2×10^5 m³. For practical applications in Taiwan as highlighted by Liu (2009), the classification of landslides is simplified to five main categories modified from Varnes (1978). These include rock falls, shallow-seated landslides, deep-seated landslides, dip-slope and wedge slides, and debris flows. Henceforth, the classification adopted in this study falls within the acceptable scheme in Taiwan.

Topographical features play an important role in determining the location and abundance of landslides (Guzzetti et al. 2008). Meunier et al. (2008), Regmi and Walter (2019), and Bhardwaj et al. (2019) have investigated the characteristics of landslides triggered by earthquakes and rainfall, and have employed different characteristics and topographical factors to analyse landslide morphology. Meunier et al. (2006), Zhuang et al. (2018), and Othman et al. (2018) suggested that landslides induced by earthquakes are concentrated near ridge crests, with over 65% originating in upper quadrant of slopes, while those induced by rainfall are often on lower slopes. Dai and Lee (2002) analysed the distribution of landslide length, width, and depth on the basis of such topographical factors as geology, lithology, elevation, slope direction and characteristics, gradient, and land use. They found the frequency of landslides to gradually increases with slope, until at about 35°–40°, beyond which it gradually decreased. In addition, the study found landslide length to increase with width or volume and concluded that landslide length had the best correlation with the change in slope. Numerous researchers have also used topographical factors in conjunction with various statistical methods, such as logistic regression (Guzzetti et al. 2008), weighting, and correlation testing to create landslide susceptibility maps (Regmi et al. 2010; Regmi and Walter 2019). Guzzetti et al. (2008) found landslides to generally occur in soft, weak rock formations with irregular layering, and the abundance of landslides increases with the landslide area, which is linked with the conclusion that
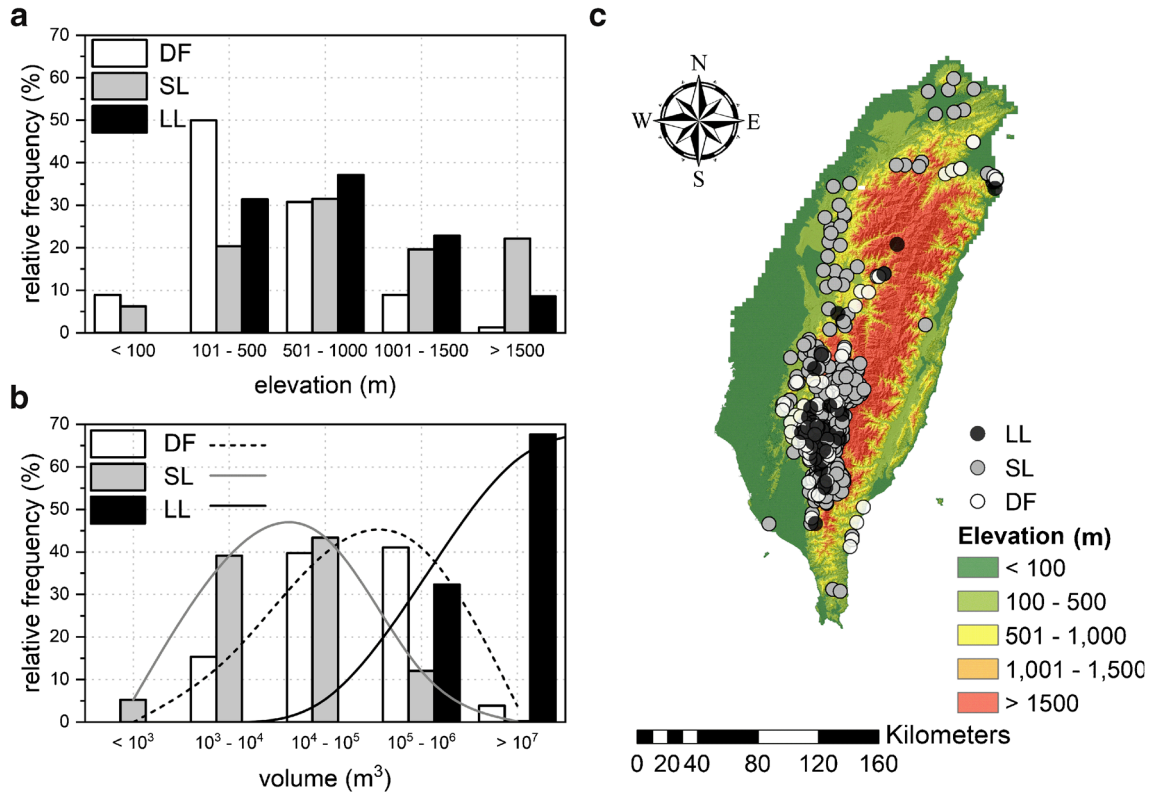
Fig. 1 Normalized frequency of landslides according to (a) elevation, (b) volume, and (c) distribution of compiled landslides

geological conditions have a very close relationship with landslide location and frequency (Cardinali et al. 2002). However, other natural conditions also have an effect on landslide location and frequency (Guzzetti et al. 2012). Besides using topographic factors, some studies have applied quantitative assessments to show important parameters in landslide mapping such as elevation, standard deviation of elevation, and slope (Lagomarsino et al. 2017). Although many papers have described landslide locations and

morphology, a little has been done on the relationship between landslide volume and morphology. Hence, this study aims to fill that gap. Additionally, the defined aimed to define some geometrical rules to characterize landslides. Landslides were first classified as SL, LL, and DF. Topographical characteristics of each were obtained for in-depth analysis. Landslide length, width, depth, volume, and area were used to draw ternary diagrams proposed
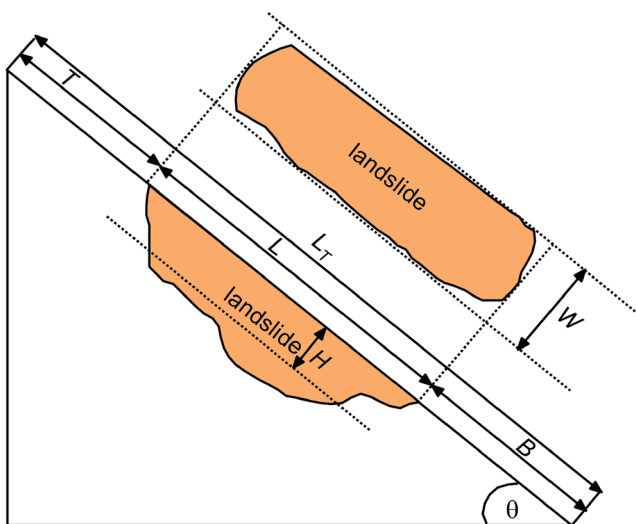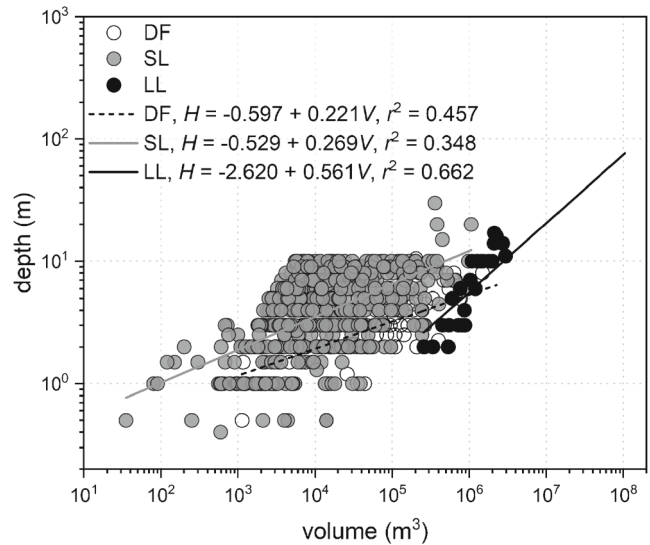

Fig. 2 Schematic diagram of the parameters used in the analysis
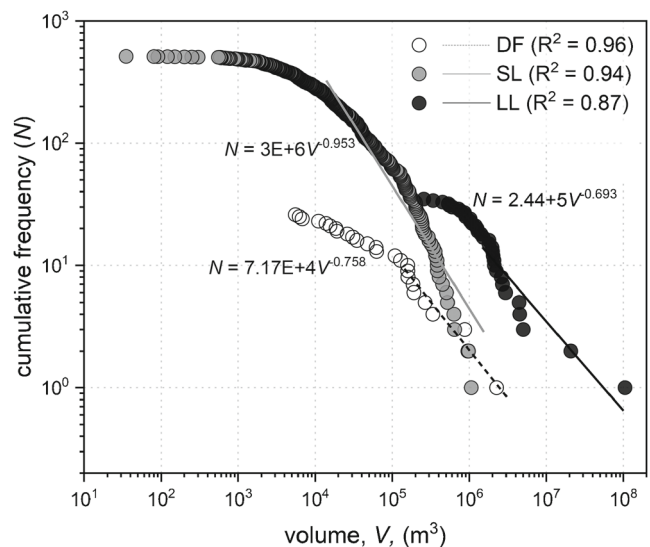
Fig. 3 Magnitude cumulative frequency curves for the landslides inventory
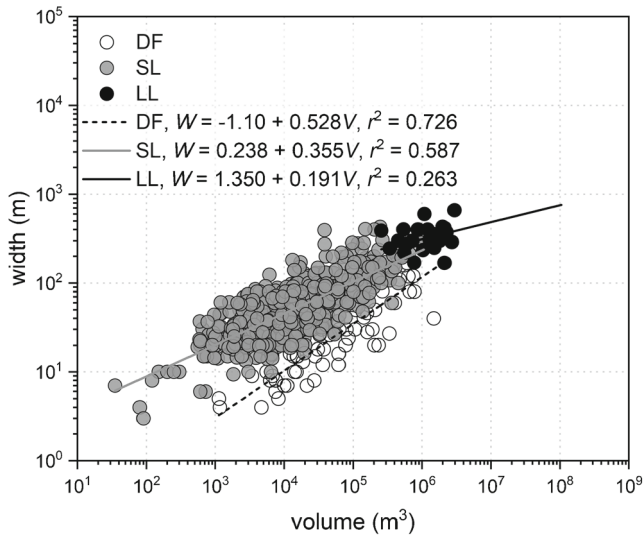
Fig. 4 Relationship between landslide width and volume

Fig. 6 Relationship between landslide depth and volume

to classify landslides in conjunction with logistic regression models.

Materials and methods

Study area

Taiwan is located on a convergent and compressive boundary along the Eurasian and Philippines sea plate, and is mainly characterized by sub-tropical and monsoon climate with plentiful rainfall. The average annual rainfall is about 2500 mm and is concentrated between May and October from typhoons and torrential rains. The country is a young orogenic belt underlain by mostly tertiary geo-synclinal sediments having a thickness of more than 10,000 m (Ho 1986). The eastern part of the island, starting from the central mountain range, is composed of metamorphic rock of the earlier Mesozoic and Palaeozoic eras. The stratum of

western Taiwan is principally made of marine rock sediment. Taiwan's strata are distributed in long and narrow strips, almost parallel to the island's axis. Sedimentary rock forms part of the island-wide piedmonts and coastal plains as well as the coastal mountain range (Ho 1986). The island is further characterized by steep terrain and river valleys, numerous mountains, large elevation differences, etc. (Fig. 1c). Mountains and hills occupy 75% of the island's area and the average slope is about 30–40%. The complex geology combined with the enormous rainfall triggers several instances of landslides (Wu et al. 2011).

Data collection and analysis

The study compiled data of landslides generated by typhoons and floods (rainfall-induced) in Taiwan between 2006 and 2014 (Fig. 1). This was mainly because rainfall influences the viscosity of the landslide mass and can almost result to maximum runout
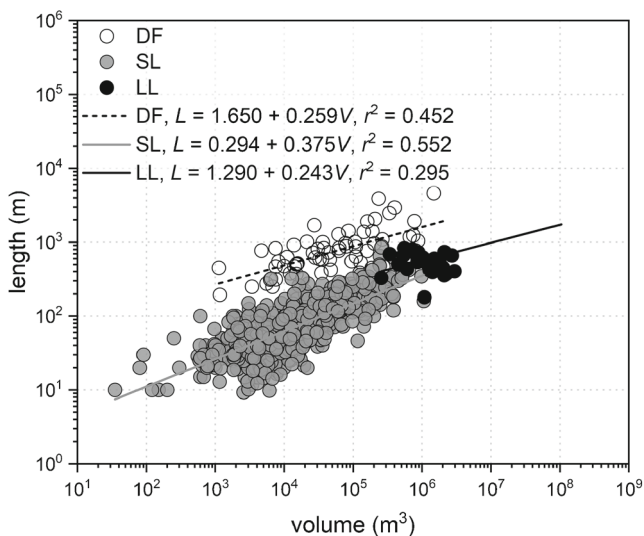
Fig. 5 Relationship between landslide length and volume
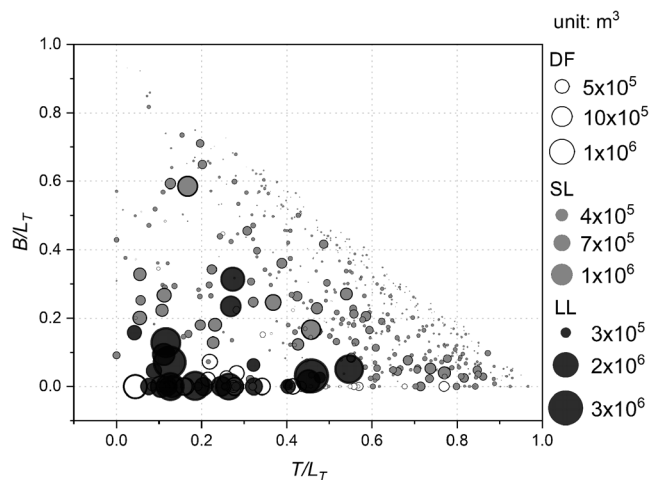
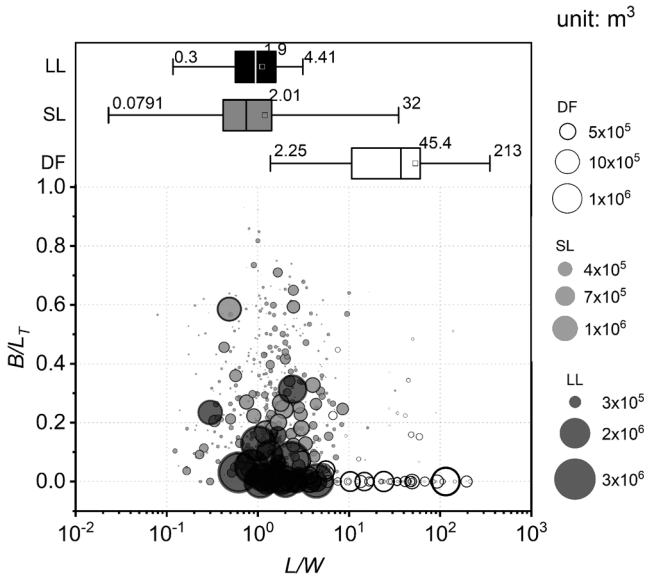**Fig. 7** Landslide location with respect to ridge crest (T/L_T) and closest stream (B/L_T)

Fig. 8 Length and width ratio (L/W) of SL, LL, and DF

Fig. 11 Characterization profile using β_1

distances. The displaced materials of a rainfall-induced landslide are usually washed away from steep slopes. It remains only the fresh scars of the rupture surface (Liu 2009) making it much simpler to afford landslide measurements. Landslide characteristics such as length (L), width (W), and mean depth (H), which are described in sections that follow and in Fig. 2, were obtained from the Taiwan official landslide website (https://246.swcb.gov.tw/Achievement/MajorDisasters). These were investigated by the Soil and Water Conservation Bureau of Taiwan through a series of investigative tools such as field measurement and aerial photos interpretation. The landslide area was computed as a product of L and W, and volume obtained through the product of this area and
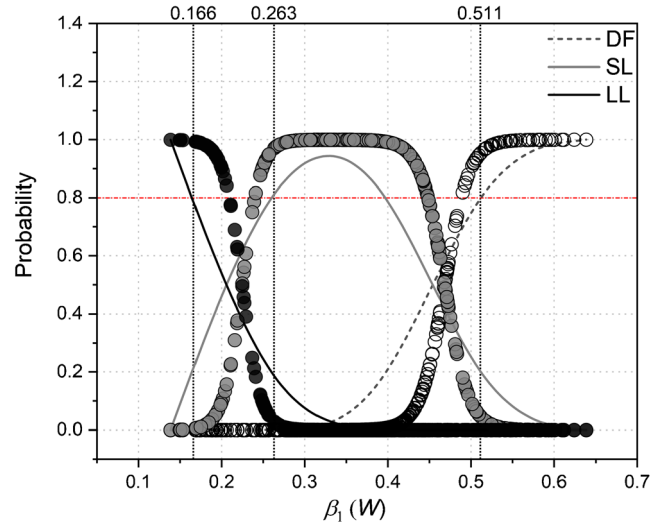
H (shown in Fig. 2). According to the definition as described in the "Introduction" section, the landslides consist 76 DF, 495 SL, and 34 LL. Their distribution is shown in Fig. 1. From the map, it can be seen that most of the landslides occurred in southern Taiwan. A study by Tsou et al. (2011) showed that this part of the island is mainly underlain by sedimentary rocks of Quaternary, Pliocene, and Miocene. This is also where the Neiying Fault is located and the combination of these attributes exposes this region to several landslide disasters.

The digital elevation model (DEM) used for the analysis was derived from a 30-m mesh Advanced Spaceborne Thermal Emission and Reflection Radiometer (ASTER) DEM. From Fig. 1, it is observed that most LL and SL occurred at an elevation > 100 m and were mostly concentrated between 500–1000 m. There were
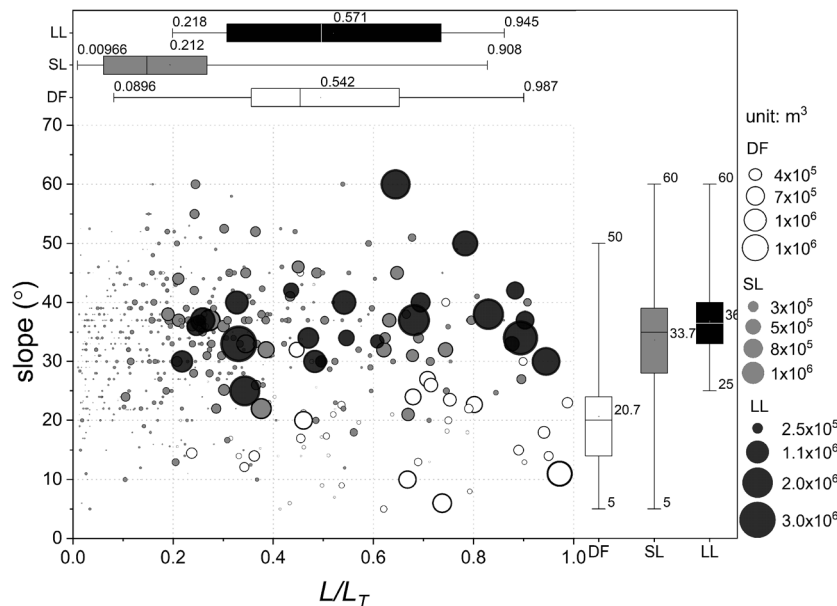

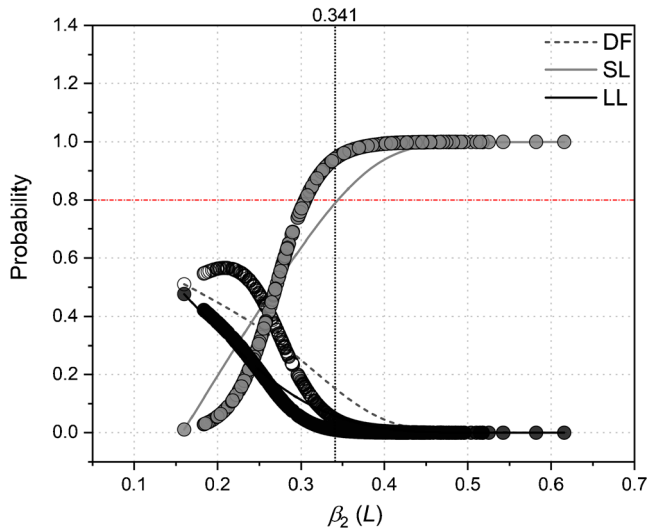**Fig. 9** The relationship between the landslide area and slope

Fig. 12 Characterization profile using β_2

Fig. 10 Ternary diagram illustrating the distribution of landslide geometry exponents

no LL at an elevation < 100 m. DF frequents were at an elevation between 100 and 500 m. The range in landslide volume for all landslides spans six orders of magnitude from 10^1 to 10^7 m³, and all LL were larger than 2×10^5 m³. Most (82%) SL ranged from 10^3–10^5 m³ as did DF. Only a few DF had volumes greater than 10^6 m³. Landslide volume from SL and DF shows near normal distributions, with an exception of LL, which shows a skewed distribution towards larger volume.

Meunier et al. (2008) characterized landslide sites in terms of their area and distribution, and found topographic site effects to have strong control over their location. Earthquake-triggered tend to be more clustered near ridge crest, while those triggered by rainfall were found mainly on colluvial slope toes. Additionally, the location of these two types gradually converged as the landslide area increased. Understanding the topographic site effects in this study requires several parameters: distance from the ridge crest to the nearest stream (L_T), ridge to the top
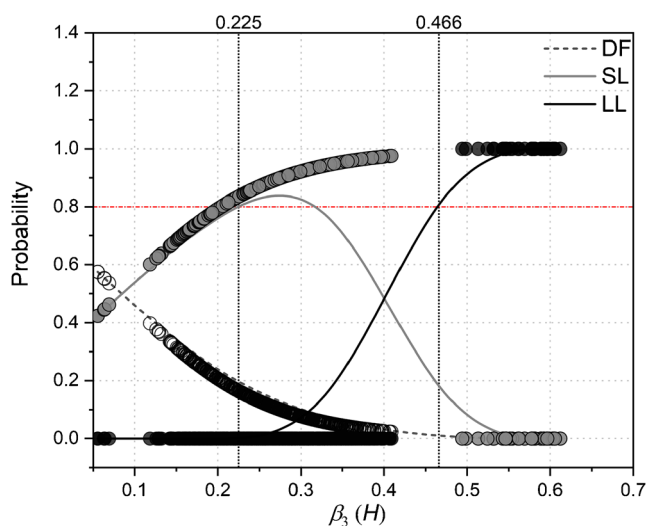
of the landslide (T), toe of the landslide to the nearest stream (B), top of the landslide to its toe (L), mean landslide depth (H), and width (tW) as illustrated by Fig. 2. These parameters were extracted from Google Earth images. The measured T and B were normalized by L_T.

Logistic regression

Logistic regression model has often been applied in the study of landslides (Lombardo and Mai 2018; Tanyas et al. 2019; Luo et al. 2019) and has provided accurate and reliable results. It is characterized by a discriminative model which estimates a probability for a given feature (Eq. 1). We applied the model to validate the ternary classification proposed, with the landslide type as our nominal response. The Akaike information criterion (AIC) (Akaike 1974) and the Bayesian information criterion (BIC) (Stone 1979) were used to evaluate the models. AIC uses the in-sample fit to estimate the likelihood of a model to predict/classify future values, while BIC measures the trade-off between model fit and complexity of the model. A better model is one that has lower AIC or BIC values. The equations (Kleinbaum 1998) below are applied;

$$p = 1 \div (1 + e^{-z}), \text{ where } z = a + b_1 X_1 + b_2 X_2 + \dots + b_n X_n \qquad (1)$$

where a is the intercept of the model, b refers to the beta values (power law scaling components of W, L, and H) associated with each of the independent variable, n is the number of variables, p is the probability varying from 0 to 1, and z varies from $-\infty$ to $+\infty$ on an S-shaped curve.

$$AIC = -2 \times \ln(L) + 2 \times k \qquad (2)$$

$$BIC = -2 \times \ln(L) + 2 \times \ln(N) \times k \qquad (3)$$

Fig. 13 Characterization profile using β_3

Table 1 Classification table for β_1

		DF	SL	LL	Correct rate (%)
	DF	65	11	0	0.855
Observed	SL	8	483	4	0.976
	LL	0	4	30	0.882
	Total (%)	0.121	0.823	0.056	0.955

where L is the value of the likelihood, N is the number of recorded measurements, and k is the number of estimated parameters.

Results and discussion

Magnitude of landslides

The magnitude cumulative frequency (MCF) analysis was derived by sorting the inventory in the order of increasing magnitude (volume) and accumulating the incremental frequencies from largest magnitude to the lowest (Hungr et al. 1999). Figure 3 shows the MCF of the 3 types of landslides, DF, SL, and LL. The empirical power law relationship between the cumulative frequency (N) and the volume (V) of DF, SL, and LL was obtained as r^2= 0.96, 0.94, and 0.87, respectively. This is in line with observation made by Tsou et al. (2017), who applied similar landslide definition as the study herein. Differences were noted however in power scaling exponents, which could be attributed to the different methodologies applied when conducting landslide inventories. Tsou et al. (2017) derived inventories from Lidar images, whereas in this study, they were derived from satellite images and ASTER DEMs. The rollover effect, where the data are no longer represented by the power law, is observed in the three landslides and is more obvious under SL and LL. Guthrie and Evans (2004) noted that larger landslides were well described by the power law, which could explain the not obvious rollover for the DF in this study.

Landslide morphology

Figures 4, 5, and 6 shows the pairs of width to volume, length to volume, and depth to volume, respectively. A majority of DF (82%) and SL (87%) had a width less than 100 m. All LL had their widths greater than 200 m with 75% clustered between 200 and 500 m. The width of DF correlated well with volume (r^2 = 0.726), while LL had the lowest correlation coefficient (r^2 = 0.263). The width of DF was significantly lower when compared with the other 2 classes. On the contrary, DF and LL had significantly higher length (> 200 m) when compared with SL, a majority of which were below 200 m. Unlike width, the regression patterns are similar with length, indicating a similar relationship with volume. A steeper

regression line is observed with LL, and stronger correlation exists between the depth and volume ($r^2 = 0.662$). The depth of SL tended to be deeper than that of DF for any given volume, and while the volume of SL increased approaching that of LL, the depth also proportionally increased.

Landslides distribution

Following the work of Meunier et al. (2008), Fig. 7 shows the location of each landslide. The normalized distance of the landslide from its top to the ridge (T/L_T: abscissa) and the normalized distance of the landslide from its toe to the nearest stream (B/L_T: ordinate) are used for the illustration. SL were concentrated on the lower-right position ($0.4 < T/L_T < 0.9$ and $0.4 < B/L_T$). This suggests that most SL occurred on lower slopes and were induced by converging runoff and stream bed erosion, similar observations made by Meunier et al. (2008), Wu et al. (2014), and Yano et al. (2019), and some are induced by river/road cutting. The presence of mechanically weak colluvial deposits and the focusing of groundwater outflow could be other attributes (Meunier et al. 2008). In contrast, DF and LL were clustered on the lower-left (Fig. 7). About 80% of DF originated in less than the upper 8/10 of the total slope length ($T/L_T < 0.8$) and extended to the streams ($B/L_T = 0$), suggesting that most DF were transported directly to rivers. Meunier et al. (2008) observed landslides triggered by typhoon Herb in 2006 that a significant portion of debris flows was delivered direct into rivers. In the population of LL, 94% extended to less than the lower 2/10 of the total slope length ($0 < B/L_T < 0.2$) whereas those extending to rivers ($B/L_T = 0$) presents 69%. Hence, most LL slided close to the stream, or even deposited rock and soil directly in the streambed suggesting high fluidity of the transported mass.

When comparing the length and width of landslides; widths of SL, LL, and DF rarely exceeded the length (i.e. L/W ratio is mostly greater than or equal to one, see Fig. 8). SL and LL had L/W ratio in the range $0.079 − 32$ and $0.3−4.41$, respectively. Comparatively, DF had a wider L/W distribution, ranging from 2.25 to 213, with more spread around the mean value of 45.7; hence, DF have more pronounced elongated form.

Table 2 Classification table for β_2

		DF	SL	LL	Correct rate (%)
	DF	42	34	0	0.553
Observed	SL	21	474	0	0.958
	LL	25	9	0	0.000
	Total (%)	0.145	0.855	0	0.853

Table 3 Classification table for β_3

		DF	SL	LL	Correct rate (%)
	DF	0	76	0	0.00
Observed	SL	5	490	0	0.99
	LL	25	9	0	1.00
	Total (%)	0.008	0.936	0.056	0.866

Landslide size and slope analysis

From Fig. 9, it can be seen that DF occurred mostly (53%) at gentler slopes (<20°). On the contrary, SL and LL were mostly concentrated on slopes >30°. About 48% of SL and 54% of LL were between 30 and 40°, an almost similar observation by Borgomeo et al. (2014). To determine the magnitude of slope failure, we used the dimensionless parameter L/L_T, which is directly proportional to the landslide area. A value of 1, therefore, would mean the failure occupied the entire slope. Figure 9 further illustrates that 88% of SL were clustered below $L/L_T = 0.4$. In selected cases, SL had $L/L_T > 0.4$ where the slope was generally short. Eighty nine percent of LL had an $L/L_T > 0.5$, some approaching 1, suggesting the entire slope to have been destroyed. Likewise, DF (85%) had $L/L_T > 0.4$ since they tended to have greater length.

Ternary distribution of landslide geometric form index

Earlier investigations have shown that in a natural river, a geometric form index relationship exists between water depth, width, and flow velocity, and formulas involving an index and coefficients have been proposed to estimate relevant factors (Leopold and Maddock 1953). Rhodes (1977) used this concept to draw the geometric form index of rivers with straight, meandering, and braided morphologies on ternary diagrams. Based on these concepts, a landslide geometric form index applicable to DF, SL, and LL is proposed. The relationship between the width (W), length (L), and depth (H) through power equations with the landslide volume (V) as the independent variable is illustrated by the equations below;

$$W = \alpha_1 V^{\beta_1} \tag{4}$$

$$L = \alpha_2 V^{\beta_2} \tag{5}$$

$$H = \alpha_3 V^{\beta_3} \tag{6}$$

Table 4 A summary statistic for logistic regression using β_1, β_2 and β_3

β	AIC	BIC	p value
β_1	136.115	153.736	0.0001
β_2	410.350	427.971	0.0001
β_3	421.759	439.380	0.0001

where α_1, α_2, and α_3 are coefficients, and β_1, β_2, and β_3 are the power law scaling exponents of W, L, and H, respectively. The βs are hereby referred to as landslide geometry exponents. The reader should note that all these coefficients and power law scaling components are empirical; hence, their values should be assessed likewise. The volume (V) can also be expressed as;

$$V = W \times L \times H \tag{7}$$

Equation 7 can be written as the following;

$$V = \alpha_1 \alpha_2 \alpha_3 V^{\beta_1 + \beta_2 + \beta_3} \tag{8}$$

Therefore, $\alpha_1 \alpha_2 \alpha_3 = 1$ and $\beta_1 + \beta_2 + \beta_3 = 1$. For graphical data presentation, β_1, β_2, β_3 are the tools for interpreting the landslide geometry.

The ternary diagram shown in Fig. 10 clearly demonstrates the differences between the three landslides observed. SL have smaller L, W, and H, and similar average β_1 and β_2. A typical SL lies almost at the centre of the ternary plot. Inversely, LL have larger L and W, and further similar averages of β_1 and β_2 to satisfy Eq. 8. This makes β_3 to be the key controlling factor for LL. A majority of the LL lie in the region with greater depth. Like LL, DF had larger L with a typical DF similar to a SL in depth (β_3). We expect the ternary plot to be universally applicable in that the different landslides within the ternary should follow the same patterns as observed in this study. Furthermore, a large database of similar scale or more would be necessary, having landslides classified as outlined in the "Introduction" section. The reader should note that the methodology was developed for rainfall-induced landslides using the database as described in the "Data collection and analysis" section. Henceforth, geological and geomorphological conditions, and role of the triggering mechanisms of landslide need to be taken into account when developing the analysis. Although, more recent techniques such as hybrid models (Luo et al. 2019) and machine learning (Dou et al. 2020) could be used, simplified tools such as the ternary plot are still necessary in practice and are still highly sought by conservation managers.

Logistic regression analysis

The ternary diagram in Fig. 10 has demonstrated the location of each landslide event and how each one may be estimated using β_1, β_2, and β_3. In an attempt to better characterize these events from β, logistic regression was applied. The characterization profiles for the different β values are shown in Figs. 11, 12, and 13. Using β_1 to classify the landslide event is shown to be applicable in all events: DF, SL, and LL. We used a probability of 0.8 (80%) as a threshold to indicate the likelihood of a landslide event. From Fig. 11, it is shown that the β_1 values for DF, SL, and LL were 0.166, 0.263, and

0.511, respectively, to get a classification with a 0.8 chance of success. Beyond 0.166, the probability (p) of correctly classifying LL in the ternary diagram is drastically reduced, while that of SL increased. Likewise, at about β_1 of 0.330, the probability of correctly classifying SL decreases, while that of DF increases. After β_1 reaches 0.511, p for DF dominates, while SL and LL are almost 0. A confusion matrix using β_1 is shown in Table 1 and the overall correct rate was 0.955.

Using β_2, shown in Fig. 12 and Table 2, suggests a threshold of 0.341 for β_2. Furthermore, this would accurately estimate SL, since beyond 0.341, the probability of DF and LL is very low (below 0.2) and is zero from $\beta_2 \sim 0.45$. This is further indicated by the poor correct rate in Table 2, where for example, the correct rate for LL was 0. There were 76 DF from our compilation; moreover, using β_2 gave only 42, having an accurate rate of 0.553.

As already indicated in the "Ternary distribution of landslide geometric form index" section, LL have larger L and W, and their β_1 and β_2 values are close to the mean, hence influencing β_3 to be the controlling factor for volume. From Fig. 13, 0.466 is the cutting point for characterizing LL. Beyond this value, p for SL nears 0, while for DF is 0. At β_3 of about 0.225, the p to correctly classify SL increases and gently decreases after β_3 of 0.3. The confusion matrix in Table 3 shows a 100% correct rate when using β_3.

A general summary of the model evaluation profiles is given by Table 4. Logistic regression using β_1 (AIC = 136.115, BIC = 153.736) outperformed both β_2 and β_3 using either AIC and BIC. The logistic model from β_3 was the poorest, having AIC and BIC values of 421.759 and 439.380, respectively. Even though some of the models performed poor, they were all significant as indicated by the p values in Table 4.

Conclusion

An improved topographic site effect method has been applied to analyse landslide's volume and characteristics. The study has also presented a ternary diagram using three indices (W (β_1), L (β_2), and H (β_3)) to develop a three-dimensional volume method of classifying landslides. Landslides were classified as debris flows, shallow, and large landslides. There was large variability in width between DF and SL, and width had a significant positive correlation with volume. The W of DF was significantly lower than that of SL and LL. DF and LL had a significantly higher L (> 200 m) when compared with SL, and a stronger correlation was found between H and volume ($r^2 = 0.662$). SL and LL had L/W ratio in the range $0.079 - 32$ and $0.3 - 4.41$, respectively. The improved topographic site effect method indicated that SL are clustered on lower slopes ($0.4 < T/L_T < 0.9$ and $0.4 < B/L_T$). LL originating from higher slopes and extending to near streams accounted for 69% of the total LL. A majority (53%) of DF occurred at slopes < 20°. To enhance the ternary diagram developed, logistic regression was applied and β_1 was found to be a better classifier of the three types of landslides (DF, SL, and LL), with a correct rate of 0.955, followed by β_3 and lastly β_2. Through characterization profiles, when using β_1, the probability (p) was 0.8 to correctly classify a landslide as LL when $\beta_1 < 0.166$, SL when $\beta_1 > 0.263$, and SL when $\beta_1 > 0.511$. AIC and BIC were the lowest for β_1 when compared with logistic models of β_2 and β_3. Moreover, β_3 logistic model had a correct rate of 100% in classifying LL. While the ternary diagram proposed in this study has been successfully applied, it is important to note that β_1, β_2, and β_3 are empirical parameters. Therefore, some deviation is expected in practice and with different regions. Nonetheless, location of the different landslides within the ternary should follow the same patterns as observed in this study, making the ternary more versatile in classifying landslides. Additionally, a large database of similar scale or more would be necessary for improved performance.

Compliance with ethical standards

Conflict of interest The authors declare that they have no conflict of interest.

References

Akaike H (1974) A new look at the statistical model identification. IEEE Trans Autom Control 19(6):716–723. https://doi.org/10.1109/TAC.1974.1100705

Bhardwaj A, Wasson RJ, Ziegler AD, Chow WT, Sundriyal YP (2019) Characteristics of rain-induced landslides in the Indian Himalaya: a case study of the Mandakini Catchment during the 2013 flood. Geomorphology 330:100–115. https://doi.org/10.1016/J.GEOMORPH.2019.01.010 URL https://www.sciencedirect.com/science/article/pii/S0169555X19 300108

Bordoni M, Valentino R, Meisina C, Bittelli M, Chersich S (2018) A simplified approach to assess the soil saturation degree and stability of a representative slope affected by shallow landslides in oltrepò pavese (Italy). Geosciences (Switzerland) 8(12), DOI https://doi.org/10.3390/geosciences8120472

Borgomeo E, Hebditch KV, Whittaker AC, Lonergan L (2014) Characterising the spatial distribution, frequency and geomorphic controls on landslide occurrence, Molise, Italy. Geomorphology 226:148–161. https://doi.org/10.1016/j.geomorph.2014.08.004

Cardinali M, Reichenbach P, Guzzetti F, Ardizzone F, Antonini G, Galli M, Cacciano M, Castellani M, Salvati P (2002) A geomorphological approach to estimate landslide hazard and risk in urban and rural areas in Umbria, central Italy. Nat Hazards Earth Syst Sci 2(1–2):57–72

Chigira M, Yagi H (2006) Geological and geomorphological characteristics of landslides triggered by the 2004 Mid Niigta prefecture earthquake in Japan. Eng Geol 82(4):202–221. https://doi.org/10.1016/J.ENGGEO.2005.10.006 URL https://www.sciencedirect.com/science/article/pii/S0013795205 002887

Cruden DM, Varnes D (1996) Landslide types and processes. Tech. rep., National Academy of Science, Washington

Dai F, Lee C (2002) Landslide characteristics and slope instability modeling using GIS, Lantau Island, Hong Kong. Geomorphology 42(3–4):213–228. https://doi.org/10.1016/S0169-555X(01)00087-3 URL https://www.sciencedirect.com/science/article/pii/S0169555X01 000873

Dille A, Kervyn F, Mugaruka Bibentyo T, Delvaux D, Ganza GB, Ilombe Mawe G, Kalikone Buzera C, Safari Nakito E, Moeyersons J, Monsieurs E, Nzolang C, Smets B, Kervyn M, Dewitte O (2019) Causes and triggers of deep-seated hillslope instability in the tropics â€ Insights from a 60-year record of Ikoma landslide (DR Congo). Geomorphology 345(106):835. https://doi.org/10.1016/J.GEOMORPH.2019.106835 URL https://www.sciencedirect.com/science/article/pii/S0169555X19 303071

Dou J, Yunus AP, Bui DT, Merghadi A, Sahana M, Zhu Z, Chen CW, Han Z, Pham BT (2020) Improved landslide assessment using support vector machine with bagging, boosting, and stacking ensemble machine learning framework in a mountainous watershed, Japan. Landslides 17(3):641–658. https://doi.org/10.1007/s10346-019-01286-5

Giannecchini R (2006) Relationship between rainfall and shallow landslides in the southern Apuan Alps (Italy). Nat Hazards Earth Syst Sci 6(3):357–364. https://doi.org/10.5194/nhess-6-357-2006

Guthrie RH, Evans SG (2004) Magnitude and frequency of landslides triggered by a storm event, Loughborough Inlet, British Columbia. Nat Hazards Earth Syst Sci 4(3):475–483. https://doi.org/10.5194/nhess-4-475-2004 URL http://www.nat-hazards-earth-syst-sci.net/4/475/2004/

Guzzetti F, Ardizzone F, Cardinali M, Galli M, Reichenbach P, Rossi M (2008) Distribution of landslides in the Upper Tiber River basin, central Italy. Geomorphology 96(1–2):105–122. https://doi.org/10.1016/J.GEOMORPH.2007.07.015 URL https://www.sciencedirect.com/science/article/pii/S0169555X07 003625

Guzzetti F, Mondini AC, Cardinali M, Fiorucci F, Santangelo M, Chang KT (2012) Landslide inventory maps: new tools for an old problem. Earth Sci Rev 112(1):42–66. https://doi.org/10.1016/j.earscirev.2012.02.001 URL http://www.sciencedirect.com/science/article/pii/S00128252120 00128

Ho CS (1986) A synthesis of the geologic evolution of Taiwan. Tectonophysics 125(1):1–16. https://doi.org/10.1016/0040-1951(86)90004-1 URL http://www.sciencedirect.com/science/article/pii/004019518690 0041

Hungr O, Evans SG, Hazzard J (1999) Magnitude and frequency of rock falls and rock slides along the main transportation corridors of southwestern British Columbia. Can Geotech J 36(2):224–238. https://doi.org/10.1139/t98-106

Hutchinson J (1988) General report: morphological and geotechnical parameters of landslides in relation to geology and hydrogeology. In: Fifth International Symposium on Landslides, pp. 3–35

Jacobs L, Dewitte O, Poesen J, Maes J, Mertens K, Sekajugo J, Kervyn M (2017) Landslide characteristics and spatial distribution in the Rwenzori Mountains, Uganda. J Afr Earth Sci 134:917–930. https://doi.org/10.1016/J.JAFREARSCI.2016.05.013 URL https://www.sciencedirect.com/science/article/pii/S1464343X16 301649

Kleinbaum DG (1998) Survival analysis, a self-learning text. Biom J 40(1):107–108. https://doi.org/10.1002/(SICI)1521-4036(199804)40:1<107::AID-BIMJ107>3.0.CO;2-9

Lagomarsino D, Tofani V, Segoni S, Catani F, Casagli N (2017) A tool for classification and regression using random forest methodology: applications to landslide susceptibility mapping and soil thickness modeling. Environ Model Assess 22(3):201–214. https://doi.org/10.1007/s10666-016-9538-y

Leopold L, Maddock T (1953) The hydraulic geometry of stream channels and some physiographic implications. Tech. rep., USGS Professional Paper

Liu JK (2009) the Geomorphometry of rainfall-induced landslides in Taiwan obtained by airborne Lidar and digital photography. IntechOpen, Rijeka, p Ch. 6, DOI https://doi.org/10.5772/8305

Lombardo L, Mai PM (2018) Presenting logistic regression-based landslide susceptibility results. Eng Geol 244:14–24. https://doi.org/10.1016/j.enggeo.2018.07.019 URL http://www.sciencedirect.com/science/article/pii/S00137952183 01212

Luo X, Lin F, Chen Y, Zhu S, Xu Z, Huo Z, Yu M, Peng J (2019) Coupling logistic model tree and random subspace to predict the landslide susceptibility areas with considering the uncertainty of environmental features. Sci Rep 9(1):15,369. https://doi.org/10.1038/s41598-019-51941-z

Meunier P, Métivier F, Lajeunesse E, Mériaux AS, Faure J (2006) Flow pattern and sediment transport in a braided river: the â€œtorrent de St Pierreâ€ (French Alps). J Hydrol 330(3–4):496–505. https://doi.org/10.1016/j.jhydrol.2006.04.009

Meunier P, Hovius N, Haines JA (2008) Topographic site effects and the location of earthquake induced landslides. Earth Planet Sci Lett 275(3-4):221–232. https://doi.org/10.1016/J.EPSL.2008.07.020 https://www.sciencedirect.com/science/article/pii/S0012821X08 004536

Othman AA, Gloaguen R, Andreani L, Rahnama M (2018) Improving landslide susceptibility mapping using morphometric features in the Mawat area, Kurdistan Region, NE Iraq: comparison of different statistical models. Geomorphology 319:147–160. https://doi.org/10.1016/J.GEOMORPH.2018.07.018 https://www.sciencedirect.com/science/article/pii/S0169555X18 302794

Regmi NR, Walter JI (2019) Detailed mapping of shallow landslides in eastern Oklahoma and western Arkansas and potential triggering by Oklahoma earthquakes. Geomorphology 106806, DOI https://doi.org/10.1016/J.GEOMORPH.2019.05.026, URL https://www.sciencedirect.com/science/article/pii/S0169555X19 301965

Regmi NR, Giardino JR, Vitek JD (2010) Modeling susceptibility to landslides using the weight of evidence approach: Western Colorado, USA. Geomorphology 115(1–2):172–187. https://doi.org/10.1016/J.GEOMORPH.2009.10.002 https://www.sciencedirect.com/science/article/pii/S0169555X09 004279

Rhodes D (1977) The b-f-m diagram; graphical representation and interpretation of at-a-station hydraulic geometry. Am J Sci 277:73–96

Santacana N, Baeza B, Corominas J, De Paz A, Marturiá J (2003) A GIS-based multivariate statistical analysis for shallow landslide susceptibility mapping in La Pobla de Lillet Area (Eastern Pyrenees, Spain). Nat Hazards 30(3):281–295. https://doi.org/10.1023/B:NHAZ.0000007169.28860.80

Stone M (1979) Comments on model selection criteria of Akaike and Schwarz. J R Stat Soc Ser B Methodol 41(2):276–278 URL http://www.jstor.org/stable/2985044

Tamura K, Uchida T, Suzuki R, Minori H, Kurihara F (2008) Evaluation of deep seated landslide susceptibility river. Tech. rep., Public Works Research Institute

Tanyas H, Rossi M, Alvioli M, van Westen CJ, Marchesini I (2019) A global slope unit-based method for the near real-time prediction of earthquake-induced landslides. Geomorphology 327:126–146. https://doi.org/10.1016/J.GEOMORPH.2018.10.022 URL https://www.sciencedirect.com/science/article/pii/S0169555X18 304367

Tsou CY, Feng ZY, Chigira M (2011) Catastrophic landslide induced by Typhoon Morakot, Shiaolin, Taiwan. Geomorphology 127(3):166–178. https://doi.org/10.1016/j.geomorph.2010.12.013 URL http://www.sciencedirect.com/science/article/pii/S0169555X100 05441

Tsou CY, Chigira M, Matsushi Y, Hiraishi N, Arai N (2017) coupling fluvial processes and landslide distribution toward geomorphological hazard assessment: a case study in a transient landscape in Japan. Landslides 14(6):1901–1914. https://doi.org/10.1007/s10346-017-0838-3

Varnes D (1978) Slope movement types and processes. In: Schuster R (ed) Landslides Control, Special Report 176

Wu CH, Chen SC, Chou HT (2011) Geomorphologic characteristics of catastrophic landslides during typhoon Morakot in the Kaoping Watershed, Taiwan. Eng Geol 123(1–2):13–21. https://doi.org/10.1016/J.ENGGEO.2011.04.018 URL https://www.sciencedirect.com/science/article/pii/S0013795211 001116

Wu CH, Chen SC, Feng ZY (2014) Formation, failure, and consequences of the Xiaolin landslide dam, triggered by extreme rainfall from Typhoon Morakot, Taiwan. Landslides 11(3):357–367. https://doi.org/10.1007/s10346-013-0394-4

Yano A, Shinohara Y, Tsunetaka H, Mizuno H, Kubota T (2019) Distribution of landslides caused by heavy rainfall events and an earthquake in northern Aso Volcano, Japan from 1955 to 2016. Geomorphology 327:533–541. https://doi.org/10.1016/J.GEOMORPH.2018.11.024 URL https://www.sciencedirect.com/science/article/pii/S0169555X18 304732

Zhuang J, Peng J, Xu C, Li Z, Densmore A, Milledge D, Iqbal J, Cui Y (2018) Distribution and characteristics of loess landslides triggered by the 1920 Haiyuan Earthquake, Northwest of China. Geomorphology 314:1–12. https://doi.org/10.1016/J.GEOMORPH.2018.04.012 URL https://www.sciencedirect.com/science/article/pii/S0169555X17 301964

S. Tfwala · C.-L. Huang
Department of Soil and Water Conservation,
National Chung Hsing University,
145 Xingda Road, 40227, Taichung City, Taiwan

S. Tfwala
e-mail: samkelet@email.nchu.edu.tw

C.-L. Huang
e-mail: judy820517@yahoo.com.tw

C.-Y. Tsou
Department of Agricultural and Environmental Engineering, Faculty of Agriculture and Life Science,
Hirosaki University,
3 Bunkyo-cho, Hirosaki, Aomori, 036-8561, Japan
e-mail: tsou.chingying@hirosaki-u.ac.jp

S.-C. Chen (✉)
Innovation and Development Centre of Sustainable Agriculture (IDCSA), Department of Soil and Water Conservation,
National Chung Hsing University,
40227, Taichung, Taiwan
Email: scchen@nchu.edu.tw